Climate Change and Hurricane-Like Extratropical Cyclones: Projections for North Atlantic Polar Lows and Medicanes Based on CMIP5 Models

R. ROMERO

Departament de Física, Universitat de les Illes Balears, Palma de Mallorca, Spain

K. EMANUEL

Department of Atmospheric Science, Massachusetts Institute of Technology, Cambridge, Massachusetts

ABSTRACT

A novel statistical–deterministic method is applied to generate thousands of synthetic tracks of North Atlantic (NA) polar lows and Mediterranean hurricanes (''medicanes''); these synthetic storms are compatible with the climates simulated by 30 CMIP5 models in both historical and RCP8.5 simulations for a recent (1986–2005) and a future (2081–2100) period, respectively. Present-to-future multimodel mean changes in storm risk are analyzed, with special attention to robust patterns (in terms of consensus among individual models) and privileging in each case the subset of models exhibiting the highest agreement with the results yielded by two reanalyses. A reduction of about 10%–15% in the overall frequency of NA polar lows that would uniformly affect the full spectrum of storm intensities is expected. In addition, a very robust regional redistribution of cases is obtained, namely a tendency to shift part of the polar low activity from the south Greenland–Icelandic sector toward the Nordic seas closer to Scandinavia. In contrast, the future change in the number of medicanes is unclear (on average the total frequency of storms does not vary), but a profound reshaping of the spectrum of lifetime maximum winds is found; the results project a higher number of moderate and violent medicanes at the expense of weak storms. Spatially, the method projects an increased occurrence of medicanes in the western Mediterranean and Black Sea that is balanced by a reduction of storm tracks in contiguous areas, particularly in the central Mediterranean; however, future extreme events (winds > 60 kt; 1 kt = 0.51 m s^{-1}) become more probable in all Mediterranean subbasins.

1. Introduction

Climate change adaptation strategies demand an analysis of the magnitude of the possible impacts on human welfare and on a variety of strategic sectors such as ecosystems, agriculture, hydrology, health, energy, and industry. An important proportion of these impacts, at least in economic cost, are produced by extreme weather–climatic phenomena (e.g., droughts, heat waves, heavy rainfall events, severe thunderstorms, and cyclonic windstorms). Among the diversity of potentially threatening cyclones, polar lows (Rasmussen and Turner 2003) and Mediterranean hurricanes, or "medicanes" (Rasmussen and Zick 1987; Reale and Atlas 2001), are two recognized

examples of mesoscale maritime extratropical storms that from a physical point of view may operate much as tropical cyclones (Emanuel and Rotunno 1989; Emanuel 2005). A visual example of a polar low and a medicane on satellite images is included in Figs. 1 and 2, respectively. Although having typical wind intensities far below those registered in their tropical analogs, both types of lows pose a serious threat to the affected islands and coastal regions and can adversely affect open sea activities such as shipping and gas and oil platforms operations.

Polar lows can be defined as maritime mesocyclones (with radii of order 100–500 km) that form at high latitudes during cold air outbreaks and are associated with intense oceanic heat fluxes and surface wind speeds in excess of $15 \, \text{m s}^{-1}$. Almost unique to the cold season, when the air–sea temperature contrast can be maximized during the cold air outbreaks over the ice-free waters, such weather systems can develop over any ocean basin in both the Northern and Southern Hemispheres, although

Corresponding author address: Departament de Física, Universitat de les Illes Balears, Cra. de Valldemossa km. 7.5, Palma de Mallorca 07122, Spain.
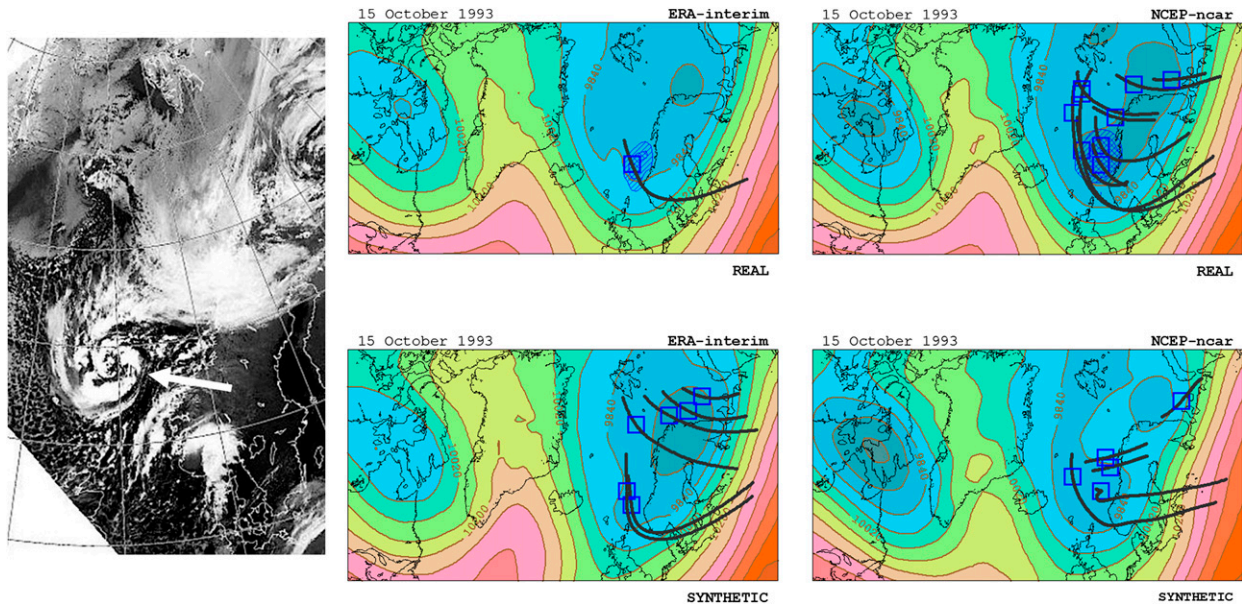E-mail: romu.romero@uib.es

FIG. 1. Synoptic scenario corresponding to the polar low "le Cygne" (NOAA/AVHRR channel 4 satellite image indicates the position of the storm at 1330 UTC 15 Oct 1993). Shown here are the daily average for that day of geopotential height at 250 hPa (contour interval 90 gpm) extracted (top) from the ERA-Interim and NCEP–NCAR reanalyses (REAL) and (bottom) from a synthetically generated analog for each reanalysis (SYNTHETIC). For each case, potential tracks identified during the episode according to the method described in the text are indicated, where the blue square on each track indicates the storm genesis location (see text). For the reanalyses, the daily average of the GEN index is also indicated (hatched area above 5 units of the index; cross-hatched area above 10 units).

North Atlantic (NA) polar lows and especially those occurring over the Norwegian and Barents Seas have received comparatively more attention in the scientific literature (e.g., Prichard 2009; Bracegirdle and Gray 2008; Zahn and von Storch 2008; Noer et al. 2011). Polar lows typically share baroclinic and surface-flux-driven dynamics; purely baroclinic, or topographically forced, systems tend to remain weak, while the development of convection seems necessary for a rapid development of an intense polar low (Renfrew 2003). In fact they are often described as Arctic "hurricanes" (Emanuel and Rotunno 1989): warm-eye structures surrounded by moist convection organized in spiral cloud bands and with the highest surface wind speeds found in the eyewall. High-resolution numerical simulations (e.g., Føre et al. 2012) confirm this thermodynamical and kinematic structure of the mature polar low and suggest that after a fundamental role of the baroclinic process and upper-level potential vorticity forcing, surface heat fluxes become increasingly important during the transition of the storm toward a wind-induced surface heat exchange (WISHE)-driven system. WISHE theory relies on the air–sea interaction instability (Emanuel 1986), which, through a positive feedback process involving surface sensible and latent heat fluxes, is ultimately manifested as the continuous latent heat release within the convective clouds responsible for the system growth. In this sense,

this mechanism can be understood as an alternative to parallel interpretations as conditional instability of the second kind (CISK) mechanism (Craig and Gray 1996).

Taken collectively, climatologies of NA polar lows are inconclusive on the average number of events annually, an important parameter for the normalization of the results presented in next sections. The reasons lie in the consideration of different geographical domains, diverse satellite- or analysis-based methods with application of rather subjective criteria and wind thresholds, and of course, the inherent difficulty of classifying cyclones that are too often manifested as hybrid systems [see Bracegirdle and Gray (2008) for an interesting discussion on these issues]. Based on intermediate calculations of cyclonic signatures obtained by Bracegirdle and Gray (2008) for the whole NA basin, and after rescaling the totals by the relative proportion of type C cyclogenesis (i.e. for which latent heat release is crucial to development) that are connected with intense surface winds, we conclude that 30 polar lows per year is an appropriate estimate for the North Atlantic. This figure is in good agreement with independent findings such as the 12 polar low events per year on average derived by Noer et al. (2011) for the Nordic Seas subsector, where about 30%–40% of the total cases should be expected according to available geographical distributions. The number of NA polar lows is expected to decrease with
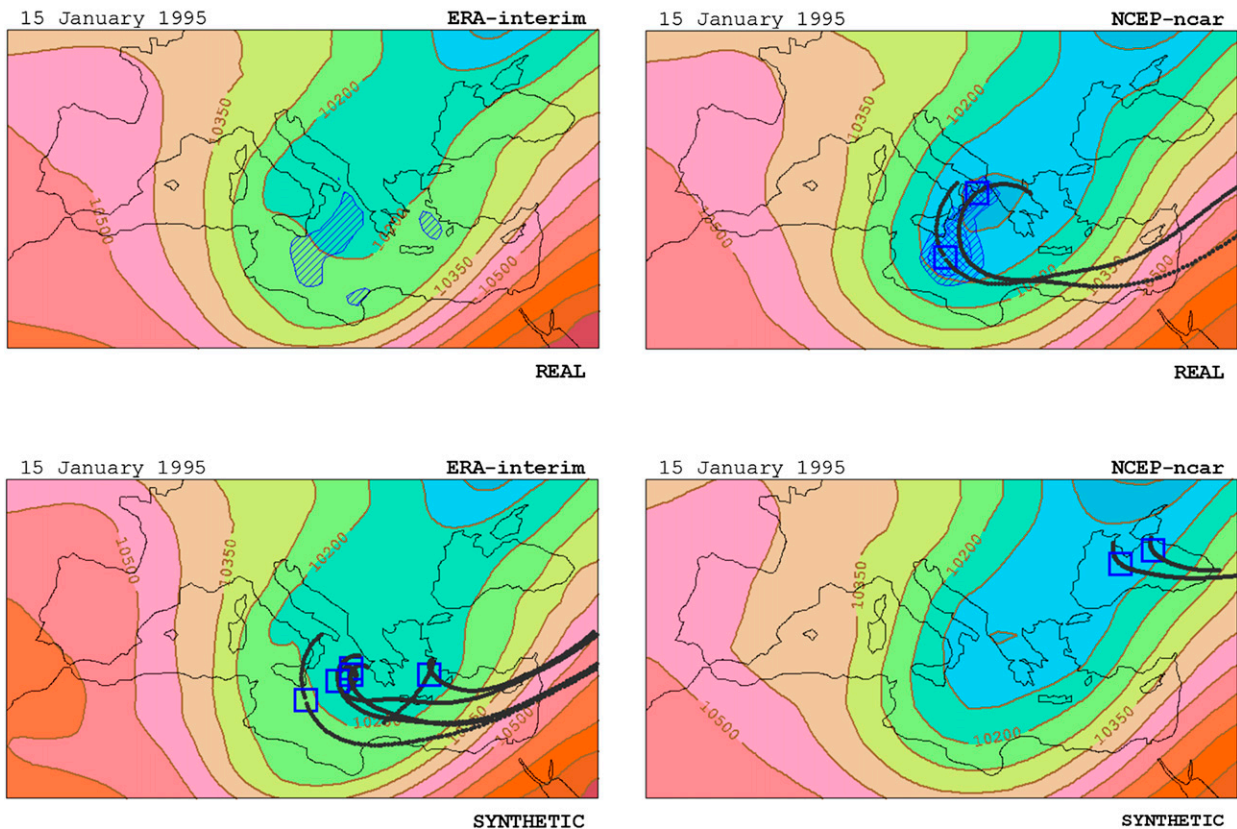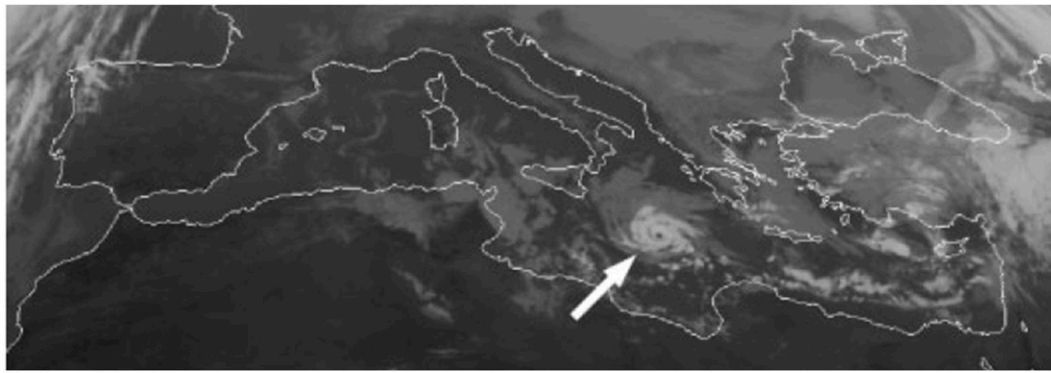
FIG. 2. Synoptic scenario corresponding to the ''Libyan'' medicane [(top) Meteosat IR channel satellite image indicates the position of the storm at 1200 UTC 16 Jan 1995]. Shown here are the daily average on 15 Jan of geopotential height at 250 hPa (contour interval 75 gpm) extracted (middle) from the ERA-Interim and NCEP–NCAR reanalyses (REAL) and (bottom) from a synthetically generated analog for each reanalysis (SYNTHETIC). For each case, potential tracks identified during the episode according to the method described in the text are indicated, where the blue square on each track indicates the storm genesis location (see text). For the reanalyses, the daily average of the GEN index is also indicated (hatched area above 5 units of the index; cross-hatched area above 10 units). (Note that ERA-Interim did not produce tracks.)

future climate warming according to Zahn and von Storch (2010), who applied a cyclone detection algorithm to dynamically downscaled results conducted with a regional climate model (RCM) nested in a global climate model (GCM) forced with four IPCC AR4 emission scenarios (C20, B1, A1B, and A2). Zahn and von Storch (2010) also projects a northward shift of the genesis regions in response to elevated atmospheric greenhouse gas concentration. These changes share some similarities with the findings of Zappa et al. (2013), who investigated the response of North Atlantic extratropical cyclones of any physical origin to

climate change as simulated by 19 GCMs participating in phase 5 of the Coupled Model Intercomparison Project (CMIP5); a slight basinwide reduction in the number of cyclones associated with strong winds was obtained. It should be noted that polar lows, owing to their small scale, are poorly represented in observational and reanalysis data (Condron et al. 2006; Zappa et al. 2014) and also in the vast majority of GCMs available today. This motivates the application of RCMs with as much resolution as possible, but the high computational cost of these tools prevents the exploration of as many present and future climate scenarios as would be desirable. Alternatively, one could explore the present-to-future changes in large-scale ingredients that under a certain range of values tend to accompany the genesis of polar lows, like the simplified vertical stability parameter of Zahn and von Storch (2010) or the marine cold air outbreak proxy parameter used in Kolstad and Bracegirdle (2008). The problem with these and other climatologically derived parameters is that they behave as necessary but not sufficient ingredients for an effective development of a polar low and that, typically, their application will only assist in answering the question about the future frequency of the phenomenon; useful projections of changes in intensity will need to rely almost exclusively on some kind of application of a numerical–physical model, given the multifaceted nature of these storms.

These problems and the resulting misrepresentation of the uncertainty of any derived climatic signal are even more exacerbated for medicanes owing to the rarity of the phenomenon; based on previous work, Romero and Emanuel (2013) estimated a frequency of two Mediterranean "hurricanes" per year on average over the same geographical domain used in this work. These cyclones share with polar lows their aesthetic appearance in satellite and radar images (as vigorous highly concentric convective cloud bands wrapped around a central eye; e.g., Moscatello et al. 2008; Tous and Romero 2013) and their warm-core and small-scale nature linked to the fundamental action of sea-to-air heat fluxes and latent heat release within the core of the storm, as revealed by numerical simulations of particular events (e.g., Lagouvardos et al. 1999; Homar et al. 2003; Tous et al. 2013). Medicanes also rely on the availability of initial dynamical forcing and the development of marked sea–atmosphere temperature contrasts; therefore a necessary—but certainly not sufficient—condition for their genesis is the approach, or development in situ, of a deep, cut-off, cold-core low in the upper and midtroposphere (Emanuel 2005; Tous and Romero 2013; Cavicchia et al. 2014a). Such a synoptic setting becomes more likely in the fall

and early winter, and thus these are the seasons exhibiting the peak medicane occurrence.

A few studies exist on the future of medicanes. Gaertner et al. (2007) used a multimodel ensemble of nine RCMs forced with a single GCM and found an enhanced future risk of "tropical" cyclone development over the Mediterranean Sea. Cavicchia et al. (2014b) reproduced for the Mediterranean the aforementioned analysis of Zahn and von Storch (2010); that is, they used a single GCM–RCM couple but three future emission scenarios and found that the projected effect of climate change on medicanes is a decreased frequency at the end of the century and a tendency toward a moderate increase of intensity with respect to the results nested within reanalysis data. Again based on a single GCM–RCM simulation system, Walsh et al. (2014) implemented a storm detection and tracking algorithm specifically designed to identify warm-core systems and suggested that the number of such systems decreases in a warmer world, particularly in winter. Tous et al. (2016) projected future changes in medicanes by making direct use of the HadGEM3 N512 high-resolution global climate model; they also found that medicanes tend to decrease in number but increase in intensity in that particular model. Romero and Emanuel (2013) went a step further and adapted for the Mediterranean the same statistical–deterministic method used here, originally devised by Emanuel (2006) for the tropical regions. This new approach entails the generation of thousands of synthetic storms with great computational efficiency and high resolution of their inner-core dynamics, thus enabling a statistically robust assessment of the current and future risk. In its original version the method has largely contributed to answer crucial questions posed during the last decade about the link between tropical cyclones and global warming, including the downscaling of CMIP5 climate models (Emanuel 2013). With regard to medicanes, Romero and Emanuel (2013) projected fewer medicanes at the end of the century in three out of the four CMIP3 models considered but a higher number of violent storms compared to present.

The present work is motivated by a concern both about the way hurricane-like extratropical cyclones could respond to global warming (e.g., possible changes in frequency, intensity, or regional variability) and the fact that no systematic effort has yet been devoted to answer these questions within the context of the CMIP5 simulations. We will revisit the problem of medicanes and will apply for the first time in the case of NA polar lows our version of the statistical–deterministic method adapted for the dynamics of mid- and high latitudes, to generate thousands of synthetic storm tracks along with their radial distributions of winds; these synthetic cyclones

will be compatible with the climates simulated by 30 CMIP5 models in both historical and RCP8.5 experiments for a recent (1986–2005) and a future (2081–2100) period, respectively.

2. Synthetic generation method and climatic datasets

Combining statistical, climate-compatible storm-track and environment generation with deterministic intensity modeling is the most crucial step of our approach toward circumventing the difficulties of assessing present and future risk using too-coarse and too-short (only decades long) climatic model outputs (Emanuel et al. 2006). But as described in Romero and Emanuel (2013), the generation of synthetic hurricane-like cyclones outside the tropics demands a redesign of the original method with regard to the production of physically sound potential tracks and concomitant kinematic and thermodynamical environments because outside the tropics the thermodynamic environment can be as variable as the kinematic environment. Once synthesized, these environments are checked for storm intensification using a simple but realistic deterministic intensity model involving both atmospheric and oceanic elements (Emanuel 1995; Emanuel et al. 2004).[1] Applications over the tropics admit a separation of time scales between the fast scale used to build the synthetic tropospheric winds and the slow scale used to define the thermodynamical environment found along the potential tracks, in both cases conforming to the climatological statistics contained in the reanalysis or GCM data (see details in Emanuel 2006). However, for mid- and high latitudes, dynamical and thermodynamical factors appear strongly interlinked and evolve in close conjunction with the movement, growth, and decay of synoptic weather systems. For that reason, we introduced a new method in which the synoptic-scale spatial and temporal variability of key ingredients for the environmental control of the storm that are needed by the intensity model (potential intensity, midtropospheric temperature and humidity, and winds in the lower and upper troposphere) is converted via principal component analysis (PCA) into a new space represented by the resulting independent PCs. Specifically, proceeding for each month separately to better account for the marked seasonalities of the North Atlantic and Mediterranean regions, we first perform a

PCA using the spatial-field correlation matrix calculated from the daily gridded fields of potential intensity (a function of SST and vertical profiles of temperature and humidity; Emanuel 1986), temperature and relative humidity at 600 hPa, and geopotential heights at 850 and 250 hPa (as surrogates of the winds via the geostrophic relation) over the geographical domains shown in Figs. 1 and 2. (For practical reasons the computations for all reanalyses and GCMs are performed using fields interpolated to a common mesh with a grid length of 75 and 50 km in these domains, respectively.) In a second step we perform a new PCA to account for the temporal structure of the data using the matrix of the time-lagged correlations among the previous "spatial–physical" PCs in each domain. For these temporal correlations we consider all the moving 10-day periods within the month (a sufficient time window to comprise any synoptic-scale evolution over the regions considered). Random draws plus slight perturbations of this final set of extracted PCs, once converted back into physical space, allow one to generate 10-day sequences of spatiotemporally coherent fields compatible with the reanalysis or GCM climate. These sequences behave as genuine analogs of truly simulated synoptic evolutions [see Romero and Emanuel (2013) for details].

To avoid the recursive simulation of unsuccessful storms, rather than determining purely at random the tracks entering the intensity model, the synthetic 10-day climate realizations are first scrutinized for the potential incubation of NA polar lows or medicanes based on physical arguments about the large-scale environments supportive of these storms. Specifically, we look for the presence of high values of an empirical index of genesis that was originally formulated by Emanuel and Nolan (2004) in the context of tropical cyclone research:

$$\mathrm{GEN} = (10^5 \eta)^{3/2} \left(\frac{\mathrm{RH}}{50}\right)^3 \left(\frac{\mathrm{PI}}{70}\right)^3 (1 + 0.1 V_{\mathrm{shear}})^{-2} \, \mathrm{m}.$$

This maritime index depends positively on potential intensity PI, absolute vorticity at low levels η (at 850 hPa), and midtropospheric relative humidity RH (at 600 hPa) and negatively on vertical wind shear across the troposphere V_{shear} (between 850 and 250 hPa). This GEN proxy parameter not only has the practical advantage of being formulated using exactly the same few fields and isobaric levels considered in the rest of the method [note that the first version of the empirical index in Emanuel and Nolan (2004) used 700 and 200 hPa to identify the mid- and upper troposphere], but it also summarizes the essence of the cold cutoff or intense mid- to upper-tropospheric trough situations that at synoptic scale drive the possible genesis of hurricane-like

---

[1] The model is axisymmetric and assumes gradient and hydrostatic balance. The square root of the absolute angular momentum per unit mass is used as the independent radial coordinate, providing very high resolution in the storm core, where it is needed.

extratropical cyclones. Under these circumstances, the air is lifted through a deep tropospheric layer, being cooled and its relative humidity increasing, inhibiting the formation of intense convective downdrafts; another disturbing factor, vertical wind shear—both directional and in magnitude—will also be limited under well-matured upper-level disturbances; and finally, the anomalously large air–sea thermodynamic disequilibrium and the cold air aloft will imply an enhanced local thermodynamic potential for "hurricanes" through the PI ingredient. The advantages of the GEN index to identify environments susceptible to medicane development have already been revealed in previous works (e.g., Tous and Romero 2013) and for the current application we also verified on several case studies of polar lows that the genesis of these Atlantic lows is simultaneous with the presence of enhanced values of the index (e.g., Fig. 1; our proxy is thus revealed as a suitable alternative to other large-scale indicators expressly designed to identify favorable conditions for polar lows; e.g., Kolstad 2011).

Specifically, in our method a possible storm genesis for both the Mediterranean and North Atlantic is implied when, within a cyclonic environment ($\eta > 10^{-4}\,\mathrm{s}^{-1}$), we detect a local maximum of GEN exceeding 10 units. [The precise values of these thresholds are basically arbitrary; in fact, Romero and Emanuel (2013) used 20 units for GEN index in their study for medicanes; after subjective examination of the typical values attained at different grid resolutions for several case studies it was here decided to halve the GEN threshold, with the aim of reducing the risk of omitting potentially good polar low/medicane environments.] From the GEN maximum locality, a candidate track is built using the weighted mean environmental flow of the 850–250-hPa tropospheric layer (a good proxy of cyclone steering current for the extratropics; e.g., Picornell et al. 2001), integrating 12 h backward in time (in order to account for the preexisting conditions) and several days forward in time, with a time step of 30 min. The meteorological parameters, bathymetry, and ocean mixed layer depth necessary for the atmospheric–oceanic numerical model simulation are obtained by interpolation along the track points (note that SST enters only through the PI definition, one of the parameters provided to the model). If this simulation along the synthetic storm track exhibits intensification to at least tropical storm force winds of 34 kt ($1\,\mathrm{kt} = 0.51\,\mathrm{m\,s}^{-1}$) or $63\,\mathrm{km\,h}^{-1}$, then a successful event is registered and the corresponding synthetic time series of storm intensity and radial distribution of wind will contribute to build the geographical probability distribution of NA polar low/medicane risk.

The ability of the method to produce dynamically consistent synoptic analogs and to recognize potential hurricane-like situations using the GEN-based criteria was tested on several episodes of storms found in the literature. For these tests and also as our reference climate in the remainder of the study we considered two reanalysis datasets of varying horizontal resolutions: ERA-Interim (Dee et al. 2011; 0.75° resolution in longitude and latitude) and NCEP–NCAR reanalysis 1 (Kalnay et al. 1996; 2.5° resolution). Two examples are displayed in Figs. 1 and 2. Figure 1 corresponds to the polar low "le Cygne" (Claud et al. 2004) that evolved over the Norwegian Sea on 13–15 October 1993, and Fig. 2 displays the "Libyan" medicane that affected the central Mediterranean waters on 15–17 January 1995 (Pytharoulis et al. 2000). For each case, the prevailing synoptic situation during the episode is illustrated through a daily average of the upper-tropospheric (250 hPa) circulation, as revealed by both reanalysis sources and by a randomly produced synthetic analog for each reanalysis. For the reanalyses we also display the simultaneous structure of the GEN-index field (note that intense local values are reached, and just for the ERA-Interim case in Fig. 2 our arbitrary threshold of 10 units is not surpassed). As expected, the synoptic scenarios of both the polar low and medicane cases are dominated by the southward intrusion of an upper-level cold trough, although many subtle differences can be detected in the circulation patterns among each of the four maps. These differences lead to considerable spread in the final number and locations of the generated potential tracks; these are shown in Figs. 1 and 2, where the blue square on each track indicates the storm genesis point identified at some time step of the dynamical evolution according to the GEN-based criteria. Typically, a highly favorable 10-day synoptic scenario will produce several potential tracks, as in some of the examples shown. Then an interesting question about the operational implementation of the method is whether we should submit all these tracks to atmospheric–oceanic model simulation or limit this final step to only a few of them (e.g., the track exhibiting the largest accumulated values of GEN along its path). We chose the first strategy; that is, we are interpreting the multiple generation of tracks in a certain synoptic environment as a powerful indicator of a higher than usual probability of hurricane-like cyclogenesis.

The method described above was applied massively using the daily data provided by the reanalyses for the period 1986–2005 and by virtually the entire set of CMIP5 models for that same period (historical scenario) and also using the model data for the future period 2081–2100, under the representative concentration pathway 8.5 (RCP8.5), a scenario of comparatively high greenhouse gas emissions (Riahi et al. 2011). The familiar

names of the 30 CMIP5 models, their horizontal resolutions, and the modeling centers/institutes on which they depend, are listed in Table 1. The GCM resolutions are consistent with the 0.75°–2.5° range spanned by the reference reanalyses, except for a few coarser models that run with grid lengths greater than 3°. It is worth mentioning that for some of the CMIP5 models more than one climatic run was available, but we only considered one per model. This is because we are more interested in examining the externally forced response of medicane and NA polar low phenomenology and in assessing the intermodel uncertainty, rather than in the internally generated variability (Power et al. 2012). Around 20 000 candidate tracks were synthetically generated over our North Atlantic domain (Fig. 1) and our Mediterranean domain (Fig. 2) from each of the 32 historical climatic datasets (reanalyses and CMIP5 models for the twentieth century), and these tracks submitted to the numerical intensity model: the absolute frequencies of successful storms (10%–40% of the initial potential tracks, depending on the model) were then normalized to the "observed" rates of 3000 and 200 storms per century (NA polar lows and medicanes, respectively; recall previous section). Finally, candidate tracks were generated and simulated for the 30 GCM projections of the future period based on the same number of 10-day synoptic realizations that was necessary to produce in the previous step for each GCM to run the historical climate; the resulting future frequencies of polar lows and medicanes were then normalized in proportion. (It should be noted that the various statistical products shown in the next section were calculated individually for each model using its full set of several thousand successful storms; the effects of the frequency normalization on these products is a simple rescaling of the calculated values for a congruent expression of the graphical results.)

3. The future of North Atlantic polar lows

The future change in the number of NA polar lows for each CMIP5 model is listed in Table 1. Both decreases and increases are obtained, ranging from halving the number of storms with respect to the present climate in several models to almost doubling the frequency in model GCM-22. Two-thirds of the models agree on a reduction of storms at the end of the century, such that the multimodel mean number of polar lows decreases from 30 storms per year in the historical scenario to 28 storms per year in the RCP8.5 scenario, a reduction of almost 7%. This negative trend in NA polar low occurrence becomes even more evident when the analysis is restricted to what we call the BEST set of models. Here we define as best models the 20 models that best reproduce

for the present climate the spatial track density of NA polar lows, compared with the reanalysis results (i.e., with the top two panels shown in Fig. 5). The goodness of the spatial distributions is quantified through the mean value of the spatial correlations with ERA-Interim and NCEP–NCAR spatial densities. This mean correlation varies from 0.65 for the worst model (GCM-22) to greater than 0.90 for models GCM-07, GCM-13, and GCM-23. Setting an arbitrary threshold value of 0.79, we keep the 20 models exhibiting a mean spatial correlation above that value (these models are indicated in Table 1; see caption). For the so defined BEST set, the future number of storms is reduced to 26 events per year (a reduction of NA polar low occurrence of almost 15% with respect to the present climate), and the model consensus on this negative trend is also enhanced (three-quarters of models agree; Table 1). For the sake of brevity, only the results corresponding to the BEST set will be shown in the following. These tend to be qualitatively similar to the products extracted from ALL models, except that higher levels in terms of model consensus (expressed as percentage of models agreeing on the present-to-future sign of change; Power et al. 2012) are generally reached.

The regional distribution of polar low genesis for three arbitrarily defined maritime areas of practically the same extent (west, central, and east; see inset in Fig. 3) is shown in Fig. 3. In the historical scenario, there is a tendency for the CMIP5 models to overestimate the frequency of storms in the central sector of the Atlantic at the expense of the western and eastern areas. The most striking feature in Fig. 3, however, is the large model consensus (>80%) in the future reduction of storms in the western and central regions but an equally likely increase in polar low genesis in the eastern part of the Atlantic. This means a west-to-east shift of NA polar low activity in spite of the total reduction of cases implied by the RCP8.5 scenario (detailed changes in the spatial distribution of storms will be discussed later).

The monthly distribution of genesis is remarkably well captured by the models (Fig. 4). As expected, the polar low phenomenology is restricted to the cold season (from October to April), but in this case the historical multimodel mean (green bar in Fig. 4) becomes more similar to the NCEP–NCAR-derived monthly values than to the ERA-Interim scenario. In fact, ERA-Interim exhibits its absolute maximum in December instead of January. Climatological studies of NA polar lows tend to exhibit the peak occurrence of storms in January and even reveal a relative minimum in February, before a recovery of activity in March (e.g., Wilhelmsen 1985; Ese et al. 1988; Noer et al. 2011). These peculiar characteristics are not

TABLE 1. List of the 30 CMIP5 models used for the downscaling of NA polar lows and medicanes. Their approximate atmospheric grid resolution for midlatitudes is indicated. The last two columns contain the mean correlation value of the track density of storms obtained in the historical scenario with that of ERA-Interim and NCEP–NCAR (first line, all correlation values are significant at $p < 0.0001$); number of storms per century in the RCP8.5 scenario, to be compared with 3000 storms per century and 200 storms per century for NA polar lows and medicanes, respectively (second line); and corresponding increase or decrease in the number of storms (arrows; with one arrow for each 10%, or fraction of 10%, of change). When the number of storms is shown with bold font, this means the corresponding CMIP5 model belongs to the BEST set (see text). The last line of the table expresses the multimodel mean of the future number of storms calculated from ALL models and for the BEST set (bold) and, in parentheses, the percentage of these models agreeing on a future decrease in the number of storms.

Modeling center (or group)	Institute ID	Model name	Lon × lat	NA POLAR LOWS	MEDICANES
Commonwealth Scientific and Industrial Research Organisation (CSIRO) and Bureau of Meteorology (BoM), Australia	CSIRO–BoM	1) ACCESS1.0	1.88° × 1.25°	0.857 ↓↓↓↓↓ **1475.3**	0.891 ↑ **209.27**
		2) ACCESS1.3	1.88° × 1.25°	0.856 ↓↓↓↓↓ **1751.5**	0.890 ↑↑ **228.95**
Beijing Climate Center, China Meteorological Administration	BCC	3) BCC_CSM1.1	2.81° × 2.79°	0.665 ↓↓↓ 2298.7	0.838 ↓ **192.58**
		4) BCC_CSM1.1(m)	1.13° × 1.12°	0.739 ↓↓↓ 2153.8	0.828 ↓↓↓↓ 136.37
College of Global Change and Earth System Science, Beijing Normal University	GCESS	5) BNU-ESM	2.81° × 2.79°	0.769 ↓↓↓↓↓ 1761.5	0.815 ↑↑↑ 259.34
Canadian Centre for Climate Modelling and Analysis	CCCma	6) CanESM2	2.81° × 2.79°	0.833 ↑ **3262.0**	0.874 ↓↓↓ **145.90**
National Center for Atmospheric Research	NCAR	7) CCSM4	1.25° × 0.94°	0.904 ↓↓ **2567.0**	0.914 ↓↓ **177.87**
Centro Euro-Mediterraneo per I Cambiamenti Climatici	CMCC	8) CMCC-CESM	3.75° × 3.71°	0.690 ↑↑↑↑↑↑ 4932.9	0.618 ↓↓↓ 159.39
		9) CMCC-CM	0.75° × 0.75°	0.794 ↑↑↑↑↑↑ **4869.7**	0.766 ↑↑ 229.27
		10) CMCC-CMS	1.88° × 1.86°	0.814 ↑ 3292.7	0.828 ↑ 215.89
Centre National de Recherches Météorologiques/Centre Européen de Recherche et de Formation Avancée en Calcul Scientifique	CNRM-CERFACS	11) CNRM-CM5	1.41° × 1.40°	0.857 ↓↓↓↓↓ **1663.8**	0.879 ↑↑↑↑ **265.92**
Commonwealth Scientific and Industrial Research Organisation in collaboration with Queensland Climate Change Centre of Excellence	CSIRO–QCCCE	12) CSIRO Mk3.6.0	1.88° × 1.86°	0.734 ↓↓↓↓↓↓↓ 1118.4	0.895 ↓↓↓↓↓↓ **78.95**
EC-EARTH consortium	EC-EARTH	13) EC-EARTH	1.13° × 1.12°	0.917 ↓↓↓ **2355.1**	0.932 ↑↑↑↑↑↑ **317.18**
LASG, Institute of Atmospheric Physics, Chinese Academy of Sciences and CESS, Tsinghua University	LASG-CESS	14) FGOALS-g2	2.81° × 2.81°	0.706 ↑↑↑↑↑↑ 4981.6	0.510 ↑↑↑↑↑ 283.64
NOAA/Geophysical Fluid Dynamics Laboratory	NOAA GFDL	15) GFDL CM3	2.50° × 2.00°	0.859 ↓↓↓ **2375.4**	0.868 ↓↓↓ **157.19**
		16) GFDL-ESM2G	2.50° × 2.00°	0.777 ↑↑↑↑ 4233.3	0.903 ↓↓ **176.53**
		17) GFDL-ESM2M	2.50° × 2.00°	0.806 ↓↓↓↓↓ **1496.3**	0.874 ↓↓↓ **142.82**

TABLE 1. (*Continued*)

Modeling center (or group)	Institute ID	Model name	Lon × lat	NA POLAR LOWS	MEDICANES
Met Office Hadley Centre	MOHC	18) HadGEM2-CC	1.88° × 1.25°	0.868	0.827
				↓↓↓↓↓ **1675.1**	↓ 190.92
Institute of Numerical Mathematics	INM	19) INM-CM4	2.00° × 1.50°	0.675	0.809
				↓↓↓↓↓ 1503.5	↓↓↓↓↓ 112.70
L'Institut Pierre-Simon Laplace	IPSL	20) IPSL-CM5A-LR	3.75° × 1.89°	0.800	0.790
				↓ **2809.2**	↑ 214.77
		21) IPSL-CM5A-MR	2.50° × 1.27°	0.858	0.850
				↓↓↓↓↓ **1706.3**	↓↓↓↓↓↓ **96.85**
		22) IPSL-CM5B-LR	3.75° × 1.89°	0.648	0.848
				↑↑↑↑↑↑↑↑↑↑ 5902.4	↑↑ 222.78
Atmosphere and Ocean Research Institute (The University of Tokyo), National Institute for Environmental Studies, and Japan Agency for Marine-Earth Science and Technology	MIROC	23) MIROC5	1.41° × 1.40°	0.925	0.894
				↓↓↓↓↓ **1504.9**	↑↑↑↑ **277.13**
		24) MIROC-ESM	2.81° × 2.79°	0.805	0.862
				↓↓ **2515.0**	↓ **192.64**
		25) MIROC-ESM-CHEM	2.81° × 2.79°	0.775	0.801
				↑ 3148.8	↓ 191.52
Max-Planck-Institut für Meteorologie (Max Planck Institute for Meteorology)	MPI-M	26) MPI-ESM-LR	1.88° × 1.86°	0.890	0.881
				↓ **2718.3**	↑↑ **223.04**
		27) MPI-ESM-MR	1.88° × 1.86°	0.896	0.900
				↓↓↓↓↓ **1675.2**	↑↑↑ **245.47**
Meteorological Research Institute	MRI	28) MRI-CGCM3	1.13° × 1.12°	0.822	0.915
				↑↑↑↑↑↑↑↑↑ 5338.4	↑ 212.25
		29) MRI-ESM1	1.13° × 1.12°	0.815	0.901
				↑↑↑↑↑↑↑ 5041.5	↑ 218.11
Norwegian Climate Centre	NCC	30) NorESM1-M	2.50° × 1.90°	0.841	0.900
				↓↓↓↓ **2066.9**	↓ **180.36**
Multimodel mean				↓ 2806.5	↓ 198.52
				(66%)	(50%)
				↓↓ **2608.0**	↓ **198.09**
				(75%)	(50%)

observed in Fig. 4, although it has to be said that the above studies focus on the area of the Atlantic near Norway. In fact, if we analyze the historical monthly distributions for the eastern region of the Atlantic exclusively (not shown), it is found that five of the GCMs (GCM-10, GCM-15, GCM-24, GCM-26, and GCM-30; all of them included in the BEST set; Table 1) plus the NCEP–NCAR reanalysis, do show the February minimum. With regard to future changes in the RCP8.5 scenario, our multimodel mean projects a decrease of polar low activity in virtually all months; as a consequence, the monthly distribution is preserved in relative terms (e.g., future maximum still occurs in January). Most of the individual models (66%–80%) agree on this reduced future probability of polar lows during all months of the year (leaving aside the irrelevant summer months; Fig. 4).

An important challenge for any downscaling technique is the ability to reproduce the observed spatial pattern of storms. We display the track density of polar lows over the North Atlantic (as a better proxy of storm risk than just genesis density), or number of storms crossing within a radius of 100 km, derived from the reanalyses and from the CMIP5 models (Fig. 5, upper panels). Some differences arise between ERA-Interim and NCEP–NCAR, but both reanalyses reproduce the main features displayed by the few compilations of events—or of genesis proxies—available for the entire basin [see Blechschmidt (2008) and Fig. 5 of Bracegirdle and Gray (2008) or Fig. 2 of Zahn and von Storch (2008)]: a maximum of storms around Iceland and the southern waters of Greenland, including cases in the Labrador Sea, and another elongated maximum off the Norway coast, including the Barents Sea. These
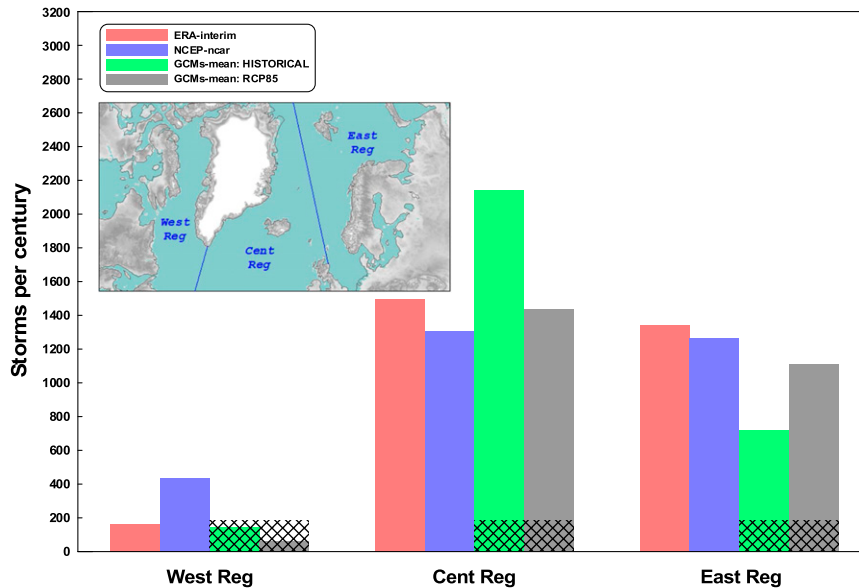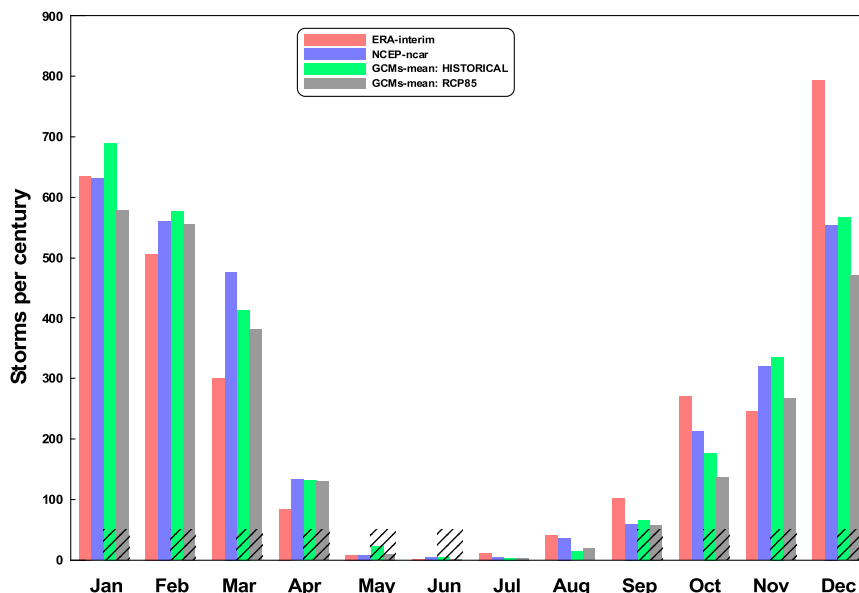
FIG. 3. Regional distribution of NA polar lows (storms per century) calculated from the reanalyses and from the set of BEST GCMs (multimodel mean; historical and RCP8.5 scenarios; see legend). For each region, the model consensus on the present-to-future sign of change at 66% and 80% levels is indicated at the base of the bars (hatched and cross-hatched areas, respectively).

features are well captured by the events downscaled from reanalyses, with a tendency in the ERA-Interim results to further emphasize the relative role of the south Icelandic maritime sector; with all, the spatial correlation between the upper two panels of Fig. 5 is very high (0.91). Even the oversmoothed track density field provided by the

CMIP5 historical multimodel mean is able to exhibit the above preferential areas (correlations with ERA-Interim and NCEP–NCAR fields are 0.93 and 0.86, respectively), although the abovementioned dipole pattern is not explicit; in fact, the geographical dipole is only clearly observed in a few CMIP5 models, but if

FIG. 4. Monthly distribution of NA polar lows (storms per century) calculated from the reanalyses and from the set of BEST GCMs (multimodel mean; historical and RCP8.5 scenarios; see legend). For each month, the model consensus on the present-to-future sign of change at 66% and 80% levels is indicated at the base of the bars (hatched and cross-hatched areas, respectively).
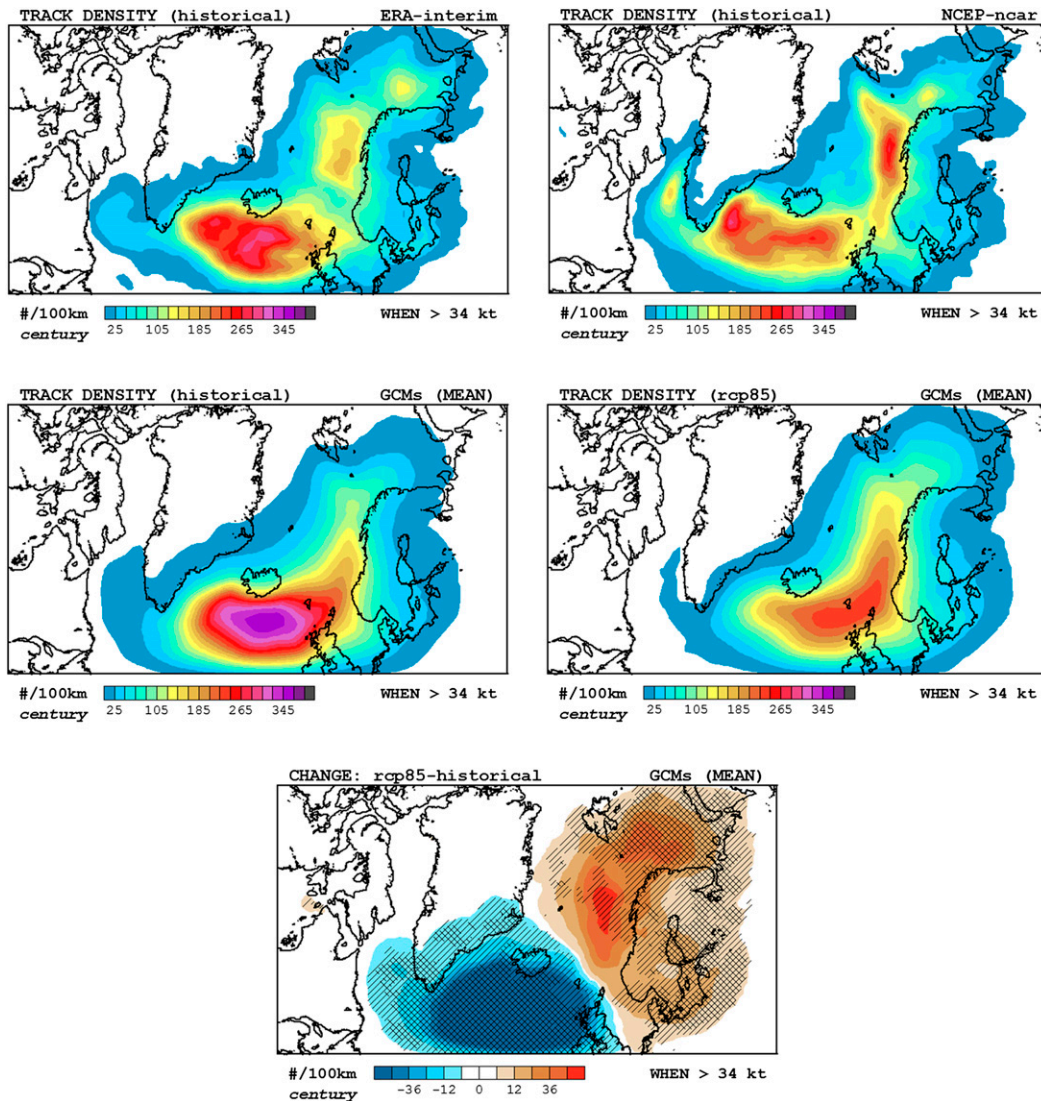
FIG. 5. NA polar low track density (storms per century within a radius of 100 km) calculated (top) from the reanalyses and (middle) from the set of BEST GCMs (multimodel mean; historical and RCP8.5 scenarios). (bottom) Present-to-future change in track density, with indications of model consensus at 66% and 80% levels (hatched and cross-hatched areas, respectively).

instead of analyzing the track density product we just consider storm genesis density (not shown), then most of individual models—and the ensemble mean—reproduce the feature. The future pattern, again summarized by means of the multimodel mean, reflects not only the decrease in the total number of polar lows but also an interesting redistribution of storm activity within the basin—namely, fewer storms in the western sector and more storms toward the northeastern Atlantic and the northern coasts of Europe. Such redistribution, already shown in bulk in Fig. 3, is more clearly illustrated through the present-to-future change in track density, a simple product included in the bottom panel of Fig. 5. This

change is complemented with the indication in Fig. 5 of the degree of model agreement on the decrease/increase of storms. With a high level of confidence, since model consensus is large and even exceeds 80% in many areas, we project a robust southwest–northeast shift of polar low activity over the North Atlantic at the end of the century. A northward shift of polar low genesis within a future context of fewer storms was also found in the downscaling work of Zahn and von Storch (2010). It is worth mentioning that we observe a very good spatial correspondence between the previously discussed regional changes in polar low activity and the present-to-future trends in the occurrence of GEN-rich environments, and when the individual
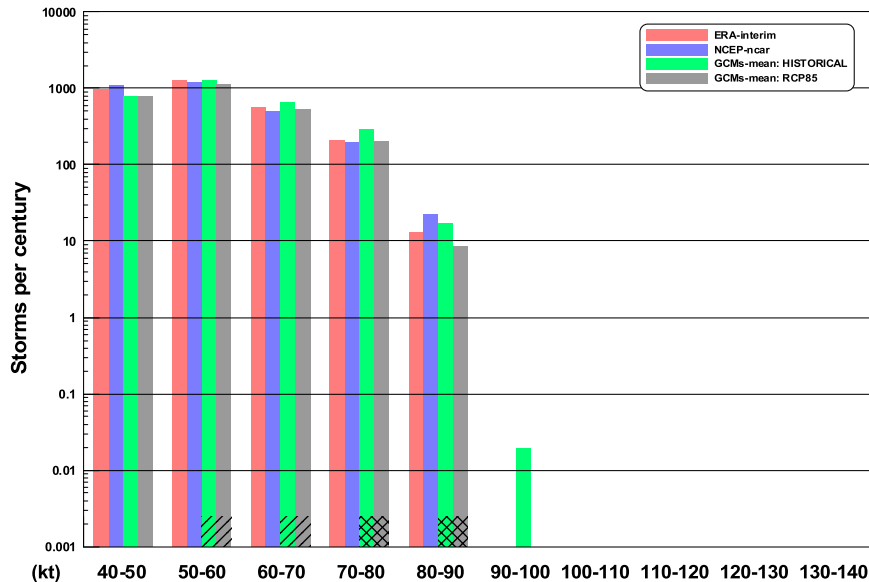
FIG. 6. Distribution of NA polar lows (storms per century; logarithmic scale) according to maximum lifetime 10-m wind of the storm (kt; horizontal axis) calculated from the reanalyses and from the set of BEST GCMs (multimodel mean; historical and RCP8.5 scenarios; see legend). For each wind class, the model consensus on the present-to-future sign of change at 66% and 80% levels is indicated at the base of the bars (hatched and cross-hatched areas, respectively).

roles of the involved physical ingredients (vorticity, humidity, potential intensity, and shear terms) are analyzed, we find that the future redistribution of storms is mostly driven by the tendencies of PI (i.e., the combined effect of changes in SST and in the frequency and intensity of cold air outbreaks) and of tropospheric wind shear; in winter PI decreases south of Greenland and Iceland and along the Norwegian coast and increases over high latitudes, and shear over the ocean becomes increasingly more favorable as we move northward (spatial maps not shown).

Polar-low-induced risks from a climatic perspective depend not only on the number of storms but also on the characteristic intensity (as measured by the wind force) associated with these events. Possible change in maximum lifetime wind of the storms at surface level is thus a critical aspect to be included in the analysis; this is done through Figs. 6 and 7. The absolute distribution of storms according to predefined extreme wind categories shows, first of all, congruent results between both reanalyses (red and blue bars in Fig. 6) and also with the present climate as seen by the CMIP5 models (green bar), except for a slight under and over population of the first and last wind classes, respectively. We note in Fig. 6 that the projected reduced number of polar lows in the RCP8.5 scenario would only affect moderate and strong wind categories (>50 kt) but not the 40–50-kt wind interval (model consensus on these changes increases as we move to the most extreme wind categories). Such reduced risk of extreme polar lows at

basin scale by the late twenty-first century is reflected in the return periods calculated for extreme maximum winds (Fig. 7). The return period curve for the RCP8.5 scenario (gray line) lies to the right of the CMIP5 historical curve (green line) for the full range of wind values, which means a lower probability of occurrence of intense polar lows in the future. Again, CMIP5 models agree on this climate change signal for a wide range of wind thresholds, even at the 80% level (see symbols on the right side of Fig. 7).

Finally, it is interesting to examine whether the reduced future risk of extreme polar lows would be a general feature of the North Atlantic or an aspect subject to regional variability, like the number of tracks. For that purpose we calculated the spatial distributions of probabilities (expressed as return periods) of reaching certain moderate to violent surface wind thresholds, a product calculated considering the radial distribution of wind of all simulated storms during their full life cycles. A representative example of the results (for a surface wind threshold of 50 kt) is displayed in Fig. 8. Besides a good correspondence between the return periods extracted from both reanalyses (Fig. 8, top panels), it is interesting to note that the likelihood of intense polar low winds is quite sensitive to latitude (these extremes are disproportionally more favored in the southern sectors of the domain in comparison with Fig. 5). Second, there is reasonable agreement between the CMIP5 multimodel historical scenario and the reanalyses, and present-to-future changes
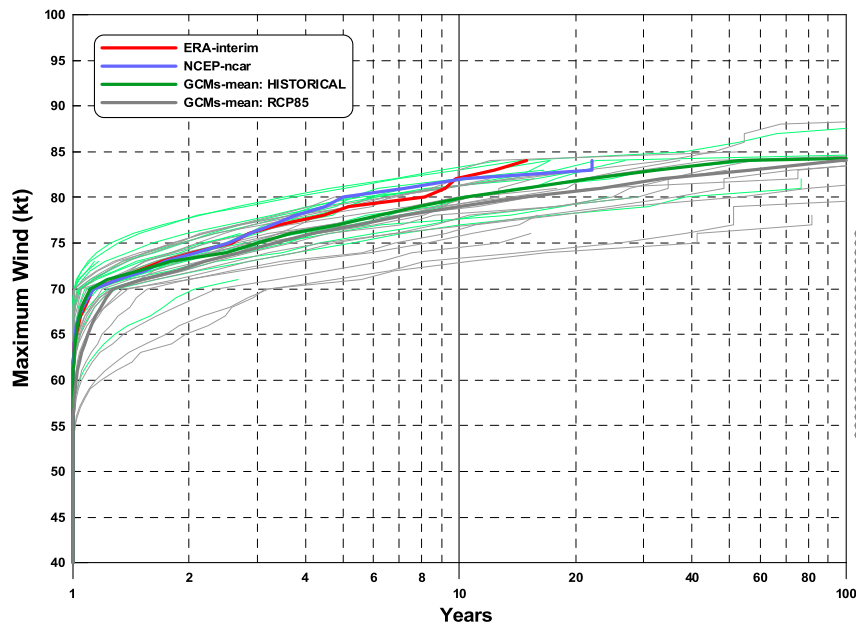
FIG. 7. Return period (yr; horizontal axis) of NA polar lows according to the maximum wind induced at the surface (kt; vertical axis) calculated from the reanalyses and from the set of BEST GCMs (multimodel mean; historical and RCP8.5 scenarios; see legend; individual models also shown as thin lines). Model consensus on the present-to-future sign of change at 66% and 80% levels is indicated along the right side of the figure.

are, in effect, regionally dependent and quite significant. Once again, we find a southwest–northeast shift of events, but this time the most affected regions would be the maritime sector south of Iceland (decrease of events) and the North Sea region and south-central Norway coasts (increase of events). Model consensus on these projected signals is very high, exceeding an 80% level in both the aforementioned regions (Fig. 8, bottom panel).

4. The future of medicanes

The results obtained for medicanes will be discussed using the same sequence of indicators that was used in the previous section to characterize the current state and future changes in storm frequency, wind intensity, and their spatial distributions. These changes seem to be qualitatively and quantitatively different for medicanes than for NA polar lows. First of all, there is great uncertainty about possible effects of climate change on the total number of medicanes. In fact, both ALL and BEST multimodel means indicate the same very slight reduction in the number of future medicanes (19.8 storms per decade vs the current frequency of 20, an insignificant reduction of only 1%). In addition, there is no model consensus on a possible reduction, as exactly 50% of models from both sets show a negative tendency in the number of medicanes (Table 1). These results contrast with previous downscaling

outputs based on just a few GCM models, which indicated a significant reduction in the future number of medicanes (e.g., Romero and Emanuel 2013; Cavicchia et al. 2014b). With regard to Table 1, it is interesting to note that four of our BEST models for medicanes (in this case, the 20 models showing a mean correlation with the reanalyses' storm-track densities greater than 0.83) were not classified within the BEST set associated with polar lows. This means that with regard to our statistical-deterministic method, the performance of the CMIP5 models depend to some degree on the region of application.

We now proceed with the analysis of the regional and monthly distributions of medicanes in the historical and RCP8.5 periods. The regional frequency of storms downscaled from the CMIP5 models over the three Mediterranean subbasins (west, central, and east) and in the neighboring Atlantic and Black Sea sectors is in general agreement with the distributions in our reference ERA-Interim and NCEP–NCAR climates (Fig. 9). The highest density of medicanes is found in the western and central Mediterranean basins, consistent with the few available databases of observed events (e.g., Tous and Romero 2013). Future changes in the regional distribution are quite modest, except for a certain agreement among individual models toward a decrease of storms in the central Mediterranean and an increase over the Black Sea (model consensus exceeds 66%; Fig. 9).
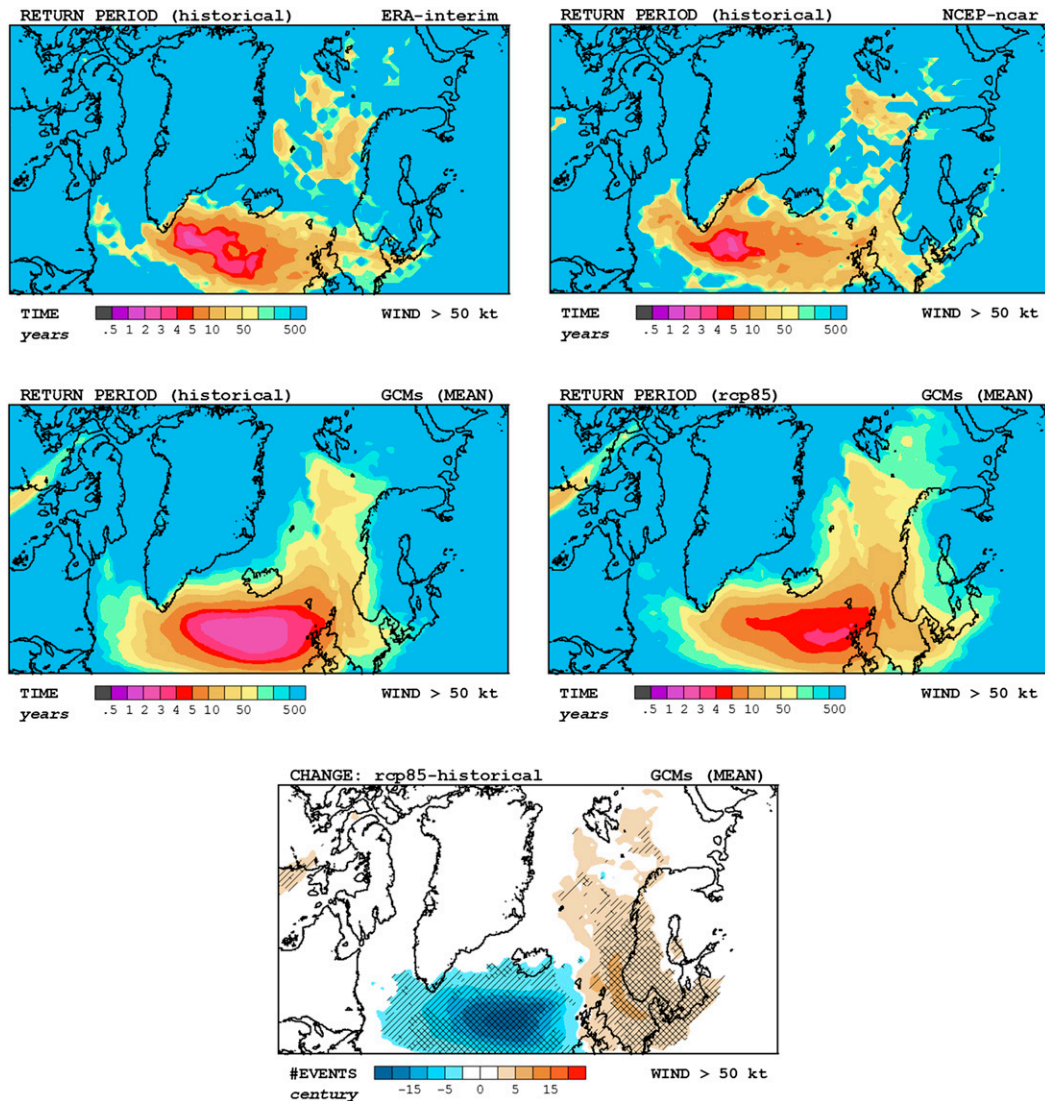
FIG. 8. Return periods (yr) for NA polar low induced surface winds above 50 kt, calculated (top) from the reanalyses and (middle) from the set of BEST GCMs (multimodel mean; historical and RCP8.5 scenarios). (bottom) Present-to-future change in the probability of these extreme winds (expressed as the change in number of events per century), with indications of model consensus at 66% and 80% levels (hatched and cross-hatched areas, respectively).

The monthly distribution of medicanes in the historical scenario (Fig. 10) is also well captured by the CMIP5 multimodel mean, being apparent in our results a strong seasonal cycle with the frequency maximum located in the fall–winter, an aspect well supported by observations (e.g., Tous and Romero 2013). Nevertheless, the high number of events obtained in August and September in the ERA-Interim scenario is noteworthy in comparison with the other reanalysis and the CMIP5 historical runs. With regard to future changes, the most interesting result is the models' tendency to develop more medicanes in the late spring and summer months (June, July, and August) and fewer cases in the late autumn and winter (from November to February). The summer increase is, however, not general in the Mediterranean; it is concentrated over the Black Sea and other northern maritime areas like the Adriatic and Gulf of Genoa (not shown); the southern areas, in spite of substantial increases of SST, remain largely unaffected by midlatitude baroclinic systems during that season, and medicanes are thereby inhibited.

Figure 11 displays in the uppermost two panels some small-scale differences between the medicane track densities calculated from both reanalyses. Even so, both historical scenarios correctly highlight the highest occurrence of medicanes in the western and central
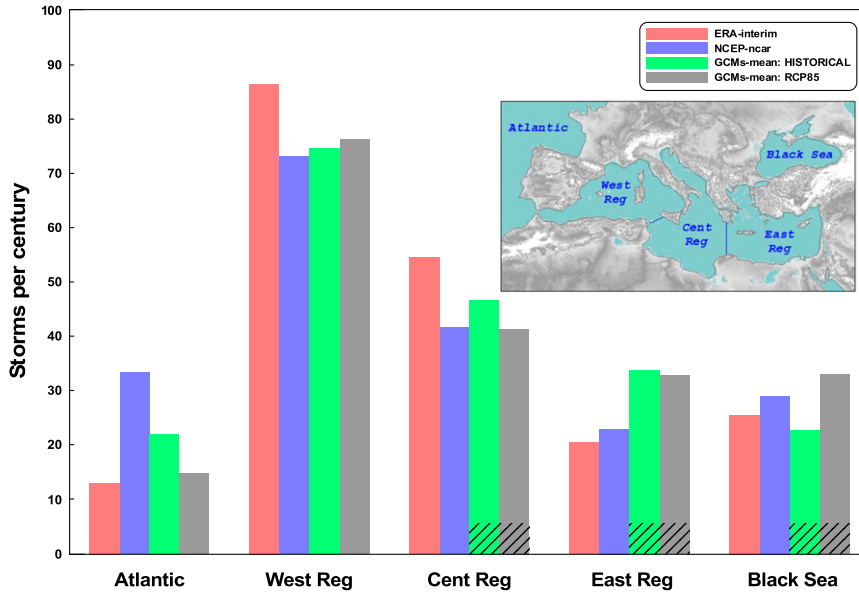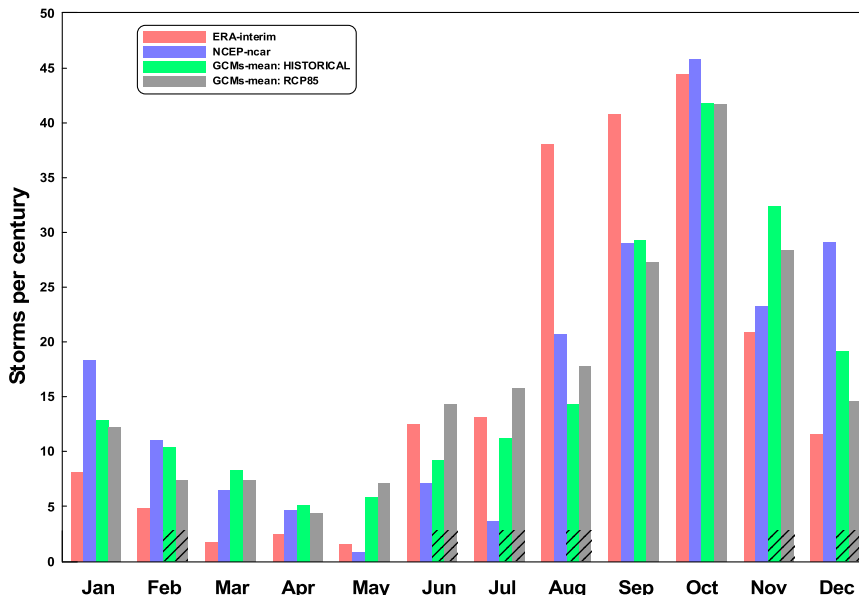
FIG. 9. Regional distribution of medicanes (storms per century) calculated from the reanalyses and from the set of BEST GCMs (multimodel mean; historical and RCP8.5 scenarios; see legend). For each region, the model consensus on the present-to-future sign of change at 66% and 80% levels is indicated at the base of the bars (hatched and cross-hatched areas, respectively).

Mediterranean and some secondary activity in the eastern Mediterranean and Black Sea; thus the density fields are well correlated with each other (correlation value is 0.86). The CMIP5 multimodel mean shown in Fig. 11 is very accurate in capturing the above spatial distribution of medicanes, with correlation values with ERA-Interim and NCEP–NCAR as high as 0.95 and 0.94, respectively. As with the NA polar lows, the regional distribution of medicane-prone conditions seems to be altered as a consequence of climate change; the RCP8.5

FIG. 10. Monthly distribution of medicanes (storms per century) calculated from the reanalyses and from the set of BEST GCMs (multimodel mean; historical and RCP8.5 scenarios; see legend). For each month, the model consensus on the present-to-future sign of change at 66% and 80% levels is indicated at the base of the bars (hatched and cross-hatched areas, respectively).
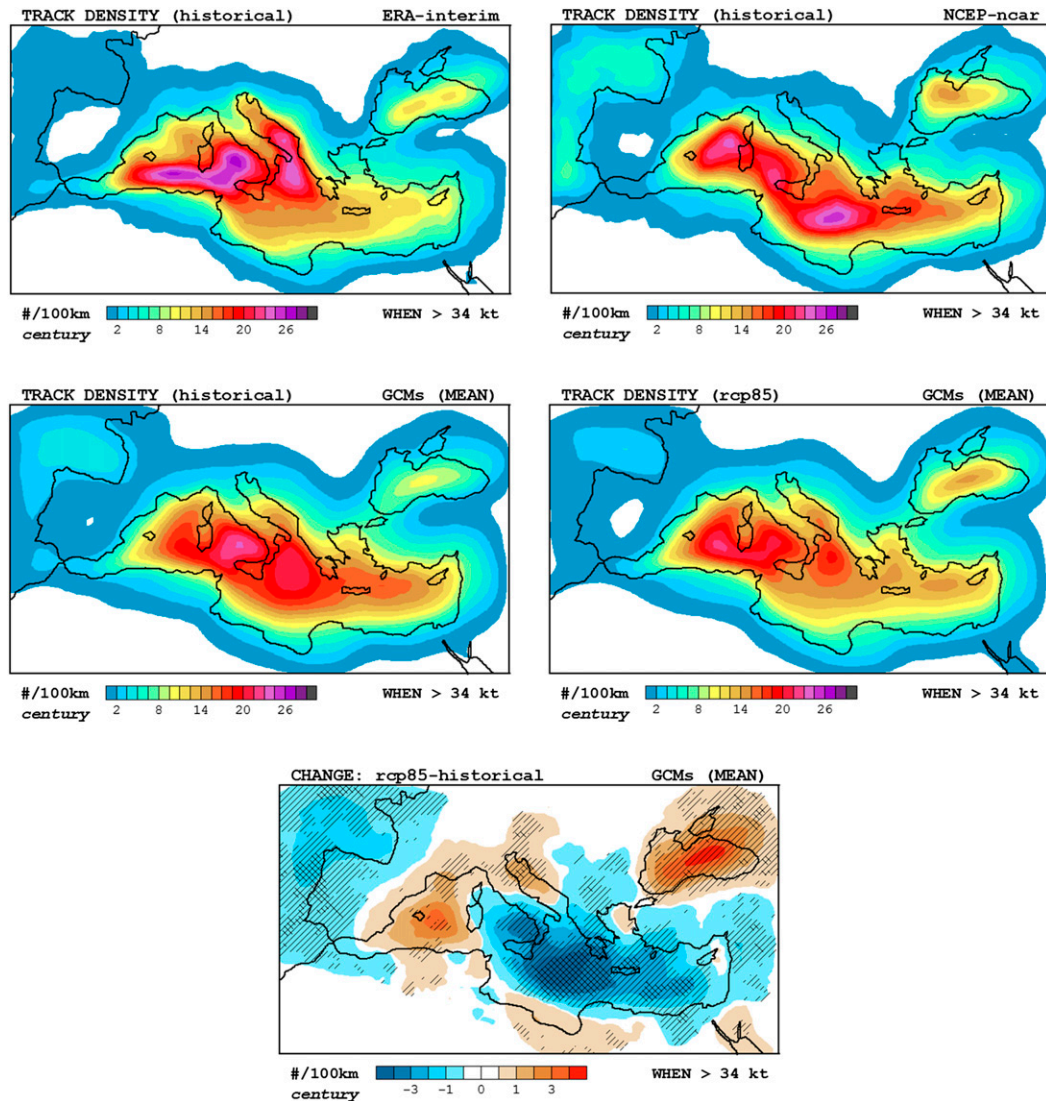
FIG. 11. Medicane track density (storms per century within a radius of 100 km) calculated from the (top) reanalyses and (middle) BEST GCMs (multimodel mean; historical and RCP8.5 scenarios). (bottom) Present-to-future change in track density, with indications of model consensus at 66% and 80% levels (hatched and cross-hatched areas, respectively).

scenario in this case produces more storms in the western Mediterranean around the Balearic Islands and over the Black Sea but fewer storms in the Atlantic sector and especially in most of the Mediterranean Sea east of Corsica and Sardinia. In fact, model consensus on these changes is low or moderate in general, but the future reduction of medicanes in a big maritime zone between southern Italy, Greece and Crete, and the African coasts is very powerful and robust in our results (more than 80% of models agree on that regional climate change signal; Fig. 11, bottom). As for polar lows, we verified that these regional changes closely overlap with the projected negative or positive trends in the occurrence of GEN-rich synoptic situations.

In this case, the general increase of PI over the warmed Mediterranean is the most critical factor in determining the sign and magnitude of these trends, as midtropospheric humidity and vertical wind shear become more hostile in the future, at least in the cold season (maps not included).

Since the number of medicanes is kept basically constant between the historical and RCP8.5 multimodel scenarios, any significant change in the distribution of storms as a function of maximum lifetime wind (Fig. 12) can be easily interpreted in terms of a possible change in the spectrum of storm intensities. Climate-change-induced redistributions of storm intensities, in the form of fewer ordinary-to-moderate events but more frequent violent
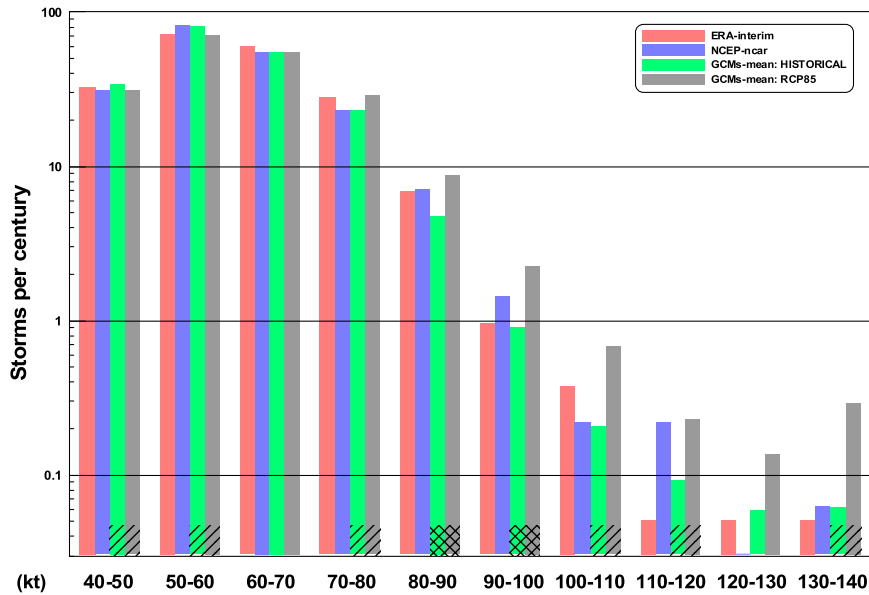
FIG. 12. Distribution of medicanes (storms per century; logarithmic scale) according to maximum lifetime 10-m wind of the storm (kt; horizontal axis) calculated from the reanalyses and from the set of BEST GCMs (multimodel mean; historical and RCP8.5 scenarios; see legend). For each wind class, the model consensus on the present-to-future sign of change at 66% and 80% levels is indicated at the base of the bars (hatched and cross-hatched areas, respectively).

cases, have already been projected in the context of tropical cyclones (e.g., Knutson and Tuleya 2004) and in previous approaches to the medicane problem (Cavicchia et al. 2014b; Tous et al. 2016; Romero and Emanuel 2013). Our results are very clear in this respect and confirm the tendency toward more violent medicanes in a warmer world; the redistribution of medicanes in Fig. 12 [future decrease (increase) of populations below (above) the 60–70-kt wind class] is moreover quite coherent among individual models, as the consensus exceeds 66% and even 80% for some wind classes. As expected, the return period curves reflect the enhanced probability of extreme medicanes in a RCP8.5 scenario (Fig. 13); the gray curve departs remarkably from the three clustered historical curves, more than doubling the future probability of very extreme storms. In addition, we find wide consensus among the CMIP5 models on the increased risk of violent medicanes as the century progresses (see symbols on the right side of Fig. 13).

Finally, it is interesting to point out that regardless of the possible rises or declines in the total number of medicanes at subregional scale (recall Fig. 11), if the analysis is restricted to extreme situations (in Fig. 14, we display, as example, return periods for surface winds above 60 kt) an increase in the risk of violent medicanes is projected over the whole Mediterranean and Black Sea. This enhanced future risk is largest over the western and central Mediterranean basins (Fig. 14, bottom), an area already exhibiting the highest probability of

extreme medicane winds according to the historical scenarios provided by the reanalyses and the CMIP5 models. Model consensus on this relevant climate change signal is at least moderate (>66%) in most of the maritime and coastal zones of the domain.

5. Conclusions

To date, most climate projections for a warmer Earth have focused on climatic mean regimes, while quantitative estimates of weather–climatic extremes at regional and local contexts are scarce. Owing to their statistical rarity, extremes are difficult to treat in climate simulations, and they often depend on poorly resolved small-scale physical processes which are subject to great uncertainty. For these reasons, weather–climatic extremes easily elude the capabilities of standard downscaling procedures, while the large cost of high-resolution simulations prevent us from considering a large ensemble of climate scenarios. This work adapted our statistical–deterministic approach to hurricane risk assessment to nontropical, surface-flux-driven storms, with the aim of assessing the current and future risk of North Atlantic polar lows and medicanes. The new method is a powerful alternative to computationally expensive classical methods (e.g., dynamical downscaling to resolve small-scale storms), with the extra benefit of producing statistically large populations of events. It was applied
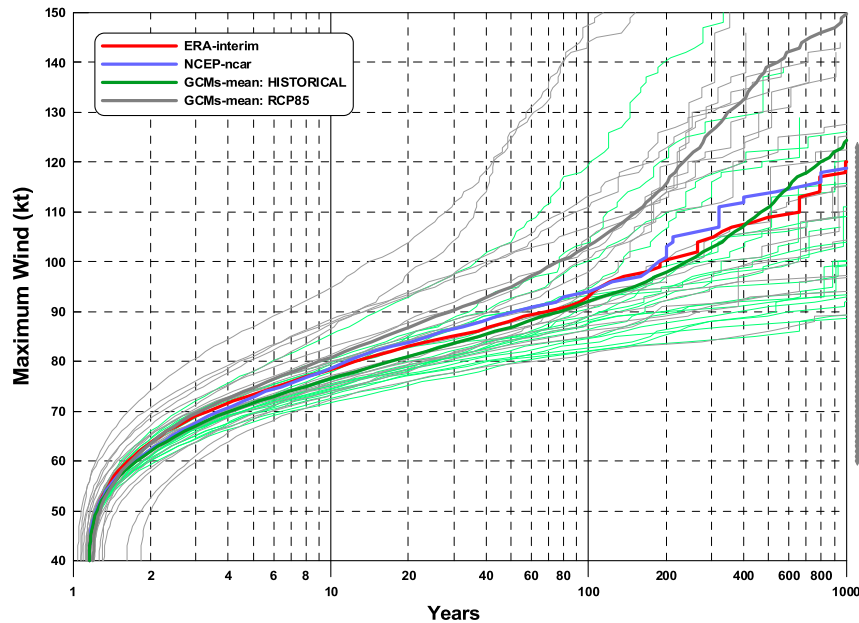
FIG. 13. Return period (yr; horizontal axis) of medicanes according to the maximum wind induced at the surface (kt; vertical axis) calculated from the reanalyses and from the set of BEST GCMs (multimodel mean; historical and RCP8.5 scenarios; see legend; individual models also shown as thin lines). Model consensus on the present-to-future sign of change at 66% and 80% levels is indicated along the right side of the figure.

to state-of-the-art historical and RCP85 scenarios of the CMIP5 global models, producing unprecedented storm and wind risk maps for the North Atlantic and Mediterranean regions. We examined the present-to-future multimodel mean changes in storm frequency and intensity, with special attention to robust patterns (in terms of the degree of consensus among individual models on the sign of change) and privileging in each case the subset of 20 models exhibiting the highest agreement with the results yielded by two reanalyses for the historical period (ERA-Interim and NCEP–NCAR).

Our main findings regarding the future of North Atlantic polar lows are as follows:

(i) We expect a reduction in the overall frequency of events that would uniformly affect the full spectrum of storm intensities over all cold season months. The annual number of NA polar lows would be lowered by 10%–15% on average with respect to the historical rate, but there is great uncertainty in the frequency change among models.

(ii) The future decrease of polar lows is far from uniform across the North Atlantic basin. Rather, a very robust regional redistribution of cases is projected—namely, a shift of polar low activity from the south Greenland–Icelandic sector toward the Nordic seas closer to Scandinavia.

(iii) Future conditions do not seem to lead to any significant variation in the relative weights of weak, moderate, and strong polar lows at basin scale. But since the number of storms is expected to decrease, we project a reduced probability of any surface wind threshold (i.e., longer return periods), considering the basin as a whole.

(iv) Again, large regional variability is expected, and while the future risk of strong polar low winds is projected to be lower in the western half of the North Atlantic, more extreme events are expected eastward, thus potentially affecting the coasts of Europe.

Our main findings regarding the future of medicanes are as follows:

(i) Future change in the number of medicanes is unclear (on average the total frequency of storms does not vary), but a profound spatial redistribution is found. Our method projects an increased occurrence of medicanes in the western Mediterranean and Black Sea, balanced by a reduction of storm tracks in contiguous areas, particularly in the central Mediterranean.

(ii) The probability of medicanes may increase during the summer while it may decrease during the late fall and winter; the probability maximum will still occur around October.
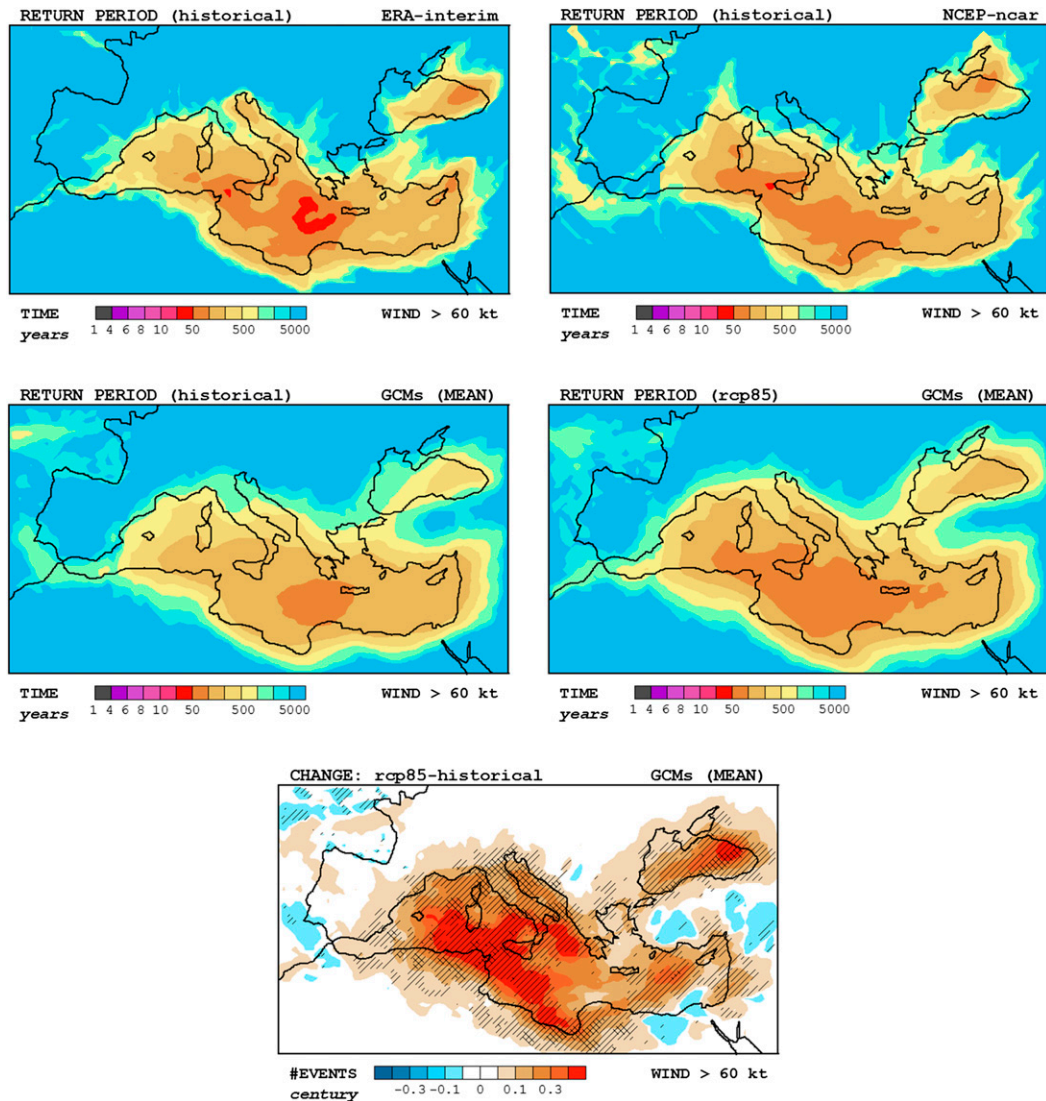
FIG. 14. Return periods (yr) for medicane-induced surface winds above 60 kt, calculated (top) from the reanalyses and (middle) from the set of BEST GCMs (multimodel mean; historical and RCP8.5 scenarios). (bottom) Present-to-future change in the probability of these extreme winds (expressed as the change in number of events per century), with indications of model consensus at 66% and 80% levels (hatched and cross-hatched areas, respectively).

(iii) We found a remarkable modification of the spectrum of lifetime maximum winds; the results project a higher number of moderate and violent medicanes at the expense of weak storms.

(iv) In particular, future extreme events (winds > 60 kt) become more likely in all Mediterranean regions, and the probability of violent medicanes (winds > 90 kt) for the basin as a whole more than doubles the current risk. As the destructive power of the storms is proportional to the wind speed cubed, these projected changes of storm intensity raise concern about the future vulnerability of Mediterranean coastal provinces.

All these projections were carried out considering the most extreme emissions pathway, RCP85, for two reasons: first, because this is the scenario with more model output available in the CMIP5 database, and second, because in our opinion a high emissions scenario currently appears as the most plausible pathway that our societies will follow during the rest of the century. Additional analyses (not shown) showed a fairly linear response of the ''hurricane''-prone environments (in a statistical sense, using the GEN proxy) to the amplitude of global warming, so we argue that the projections for both NA polar lows and medicanes under other commonly considered scenarios (e.g., RCP2.6 and RCP4.5) would be found part

way between our historical and RCP8.5 results. Finally, we believe that research on the future of hurricane-like extratropical cyclones using this and other techniques will remain very active in the following years in step with the constant flow of new global climate simulations, although in our experience the diversity of model responses at regional and subregional scale will continue to be high. Since the potential intensity of the environment is a critical factor for the genesis and physical operation of these cyclones, future improvements in the quality and resolution of thermodynamic fields for coastal and interior seas will particularly benefit the new calculations and impact assessments.

REFERENCES

Blechschmidt, A.-M., 2008: A 2-year climatology of polar low events over the Nordic seas from satellite remote sensing. *Geophys. Res. Lett.*, **35**, L09815, doi:10.1029/2008GL033706.

Bracegirdle, T. J., and S. L. Gray, 2008: An objective climatology of the dynamical forcing of polar lows in the Nordic seas. *Int. J. Climatol.*, **28**, 1903–1919, doi:10.1002/joc.1686.

Cavicchia, L., H. von Storch, and S. Gualdi, 2014a: A long-term climatology of medicanes. *Climate Dyn.*, **43**, 1183–1195, doi:10.1007/s00382-013-1893-7.

——, ——, and ——, 2014b: Mediterranean tropical-like cyclones in present and future climate. *J. Climate*, **27**, 7493–7501, doi:10.1175/JCLI-D-14-00339.1.

Claud, C., G. Heinemann, E. Raustein, and L. Mcmurdie, 2004: Polar low le Cygne: Satellite observations and numerical simulations. *Quart. J. Roy. Meteor. Soc.*, **130**, 1075–1102, doi:10.1256/qj.03.72.

Condron, A., G. R. Bigg, and I. A. Renfrew, 2006: Polar mesoscale cyclones in the northeast Atlantic: Comparing climatologies from ERA-40 and satellite imagery. *Mon. Wea. Rev.*, **134**, 1518–1533, doi:10.1175/MWR3136.1.

Craig, G. C., and S. L. Gray, 1996: CISK or WISHE as the mechanism for tropical cyclone intensification. *J. Atmos. Sci.*, **53**, 3528–3540, doi:10.1175/1520-0469(1996)053<3528: COWATM>2.0.CO;2.

Dee, D. P., and Coauthors, 2011: The ERA-Interim reanalysis: Configuration and performance of the data assimilation system. *Quart. J. Roy. Meteor. Soc.*, **137**, 553–597, doi:10.1002/qj.828.

Emanuel, K. A., 1986: An air–sea interaction theory for tropical cyclones. Part I: Steady-state maintenance. *J. Atmos. Sci.*, **43**, 585–604, doi:10.1175/1520-0469(1986)043<0585: AASITF>2.0.CO;2.

——, 1995: The behavior of a simple hurricane model using a convective scheme based on subcloud-layer entropy equilibrium. *J. Atmos. Sci.*, **52**, 3960–3968, doi:10.1175/ 1520-0469(1995)052<3960:TBOASH>2.0.CO;2.

——, 2005: Genesis and maintenance of "Mediterranean hurricanes." *Adv. Geosci.*, **2**, 217–220, doi:10.5194/adgeo-2-217-2005.

——, 2006: Climate and tropical cyclone activity: A new model downscaling approach. *J. Climate*, **19**, 4797–4802, doi:10.1175/ JCLI3908.1.

——, 2013: Downscaling CMIP5 climate models shows increased tropical cyclone activity over the 21st century. *Proc. Natl. Acad. Sci. USA*, **110**, 12 219–12 224, doi:10.1073/pnas.1301293110.

——, and R. Rotunno, 1989: Polar lows as Arctic hurricanes. *Tellus*, **41A**, 1–17, doi:10.1111/j.1600-0870.1989.tb00362.x.

——, and D. S. Nolan, 2004: Tropical cyclone activity and the global climate system. *26th Conf. on Hurricanes and Tropical Meteorology*, Miami, FL, Amer. Meteor. Soc., 10A.2. [Available online at https://ams.confex.com/ams/26HURR/techprogram/paper_ 75463.htm.]

——, C. DesAutels, C. Holloway, and R. Korty, 2004: Environmental control of tropical cyclone intensity. *J. Atmos. Sci.*, **61**, 843–858, doi:10.1175/1520-0469(2004)061<0843:ECOTCI>2.0.CO;2.

——, S. Ravela, E. Vivant, and C. Risi, 2006: A statistical deterministic approach to hurricane risk assessment. *Bull. Amer. Meteor. Soc.*, **87**, 299–314, doi:10.1175/BAMS-87-3-299.

Ese, T., I. Kanestrøm, and K. Pedersen, 1988: Climatology of polar lows over the Norwegian and Barents Seas. *Tellus*, **40A**, 248–255, doi:10.1111/j.1600-0870.1988.tb00345.x.

Føre, I., J. E. Kristjánsson, E. W. Kolstad, T. J. Bracegirdle, Ø. Saetra, and B. Røsting, 2012: A 'hurricane-like' polar low fuelled by sensible heat flux: High-resolution numerical simulations. *Quart. J. Roy. Meteor. Soc.*, **138**, 1308–1324, doi:10.1002/qj.1876.

Gaertner, M. A., D. Jacob, V. Gil, M. Domínguez, E. Padorno, E. Sánchez, and M. Castro, 2007: Tropical cyclones over the Mediterranean Sea in climate change simulations. *Geophys. Res. Lett.*, **34**, L14711, doi:10.1029/2007GL029977.

Homar, V., R. Romero, D. J. Stensrud, C. Ramis, and S. Alonso, 2003: Numerical diagnosis of a small, quasi-tropical cyclone over the western Mediterranean: Dynamical vs. boundary factors. *Quart. J. Roy. Meteor. Soc.*, **129**, 1469–1490, doi:10.1256/ qj.01.91.

Kalnay, E., and Coauthors, 1996: The NCEP/NCAR 40-Year Reanalysis Project. *Bull. Amer. Meteor. Soc.*, **77**, 437–471, doi:10.1175/1520-0477(1996)077<0437:TNYRP>2.0.CO;2.

Knutson, T. R., and R. E. Tuleya, 2004: Impact of CO_2-induced warming on simulated hurricane intensity and precipitation: Sensitivity to the choice of climate model and convective parameterization. *J. Climate*, **17**, 3477–3495, doi:10.1175/ 1520-0442(2004)017<3477:IOCWOS>2.0.CO;2.

Kolstad, E. W., 2011: A global climatology of favourable conditions for polar lows. *Quart. J. Roy. Meteor. Soc.*, **137**, 1749–1761, doi:10.1002/qj.888.

——, and T. J. Bracegirdle, 2008: Marine cold-air outbreaks in the future: An assessment of IPCC AR4 model results for the Northern Hemisphere. *Climate Dyn.*, **30**, 871–885, doi:10.1007/s00382-007-0331-0.

Lagouvardos, K., V. Kotroni, S. Nickovic, D. Jovic, G. Kallos, and C. J. Tremback, 1999: Observations and model simulations of a winter sub-synoptic vortex over the central Mediterranean. *Meteor. Appl.*, **6**, 371–383, doi:10.1017/S1350482799001309.

Moscatello, A., M. M. Miglietta, and R. Rotunno, 2008: Observational analysis of a Mediterranean 'hurricane' over southeastern Italy. *Weather*, **63**, 306–311, doi:10.1002/wea.231.

Noer, G., Ø. Saetra, T. Lien, and Y. Gusdal, 2011: A climatological study of polar lows in the Nordic seas. *Quart. J. Roy. Meteor. Soc.*, **137**, 1762–1772, doi:10.1002/qj.846.

Picornell, M. A., A. Jansà, A. Genovés, and J. Campins, 2001: Automated database of mesocyclones from the HIRLAM(INM)-0.5° analyses in the western Mediterranean. *Int. J. Climatol.*, **21**, 335–354, doi:10.1002/joc.621.

Power, S. B., F. Delage, R. Colman, and A. Moise, 2012: Consensus on twenty-first-century rainfall projections in climate models more widespread than previously thought. *J. Climate*, **25**, 3792–3809, doi:10.1175/JCLI-D-11-00354.1.

Prichard, B., 2009: A late October polar low. *Weather*, **64**, 270–273, doi:10.1002/wea.437.

Pytharoulis, I., G. C. Craig, and S. P. Ballard, 2000: The hurricane-like Mediterranean cyclone of January 1995. *Meteor. Appl.*, **7**, 261–279, doi:10.1017/S1350482700001511.

Rasmussen, E., and C. Zick, 1987: A subsynoptic vortex over the Mediterranean with some resemblance to polar lows. *Tellus*, **39A**, 408–425, doi:10.1111/j.1600-0870.1987.tb00318.x.

——, and J. Turner, Eds., 2003: *Polar Lows: Mesoscale Weather Systems in the Polar Regions*. Cambridge University Press, 612 pp.

Reale, O., and R. Atlas, 2001: Tropical cyclone–like vortices in the extratropics: Observational evidence and synoptic analysis. *Wea. Forecasting*, **16**, 7–34, doi:10.1175/1520-0434(2001)016<0007:TCLVIT>2.0.CO;2.

Renfrew, I. A., 2003: Polar lows. *Encyclopedia of Atmospheric Sciences*, J. R. Holton, J. A. Curry, and J. A. Pyle, Eds., Vol. 3, Academic Press, 1761–1768, doi:10.1016/B0-12-227090-8/00317-1.

Riahi, K., and Coauthors, 2011: RCP 8.5—A scenario of comparatively high greenhouse gas emissions. *Climatic Change*, **109**, 33–57, doi:10.1007/s10584-011-0149-y.

Romero, R., and K. Emanuel, 2013: Medicane risk in a changing climate. *J. Geophys. Res. Atmos.*, **118**, 5992–6001, doi:10.1002/jgrd.50475.

Tous, M., and R. Romero, 2013: Meteorological environments associated with medicane development. *Int. J. Climatol.*, **33**, 1–14, doi:10.1002/joc.3428.

——, ——, and C. Ramis, 2013: Surface heat fluxes influence on medicane trajectories and intensification. *Atmos. Res.*, **123**, 400–411, doi:10.1016/j.atmosres.2012.05.022.

——, G. Zappa, R. Romero, L. Shaffrey, and P. L. Vidale, 2016: Projected changes in medicanes in the HadGEM3 N512 high-resolution global climate model. *Climate Dyn.*, **47**, 1913–1924, doi:10.1007/s00382-015-2941-2.

Walsh, K., F. Giorgi, and E. Coppola, 2014: Mediterranean warm-core cyclones in a warmer world. *Climate Dyn.*, **42**, 1053–1066, doi:10.1007/s00382-013-1723-y.

Wilhelmsen, K., 1985: Climatological study of gale-producing polar lows near Norway. *Tellus*, **37A**, 451–459, doi:10.1111/j.1600-0870.1985.tb00443.x.

Zahn, M., and H. von Storch, 2008: A long-term climatology of North Atlantic polar lows. *Geophys. Res. Lett.*, **35**, L22702, doi:10.1029/2008GL035769.

——, and ——, 2010: Decreased frequency of North Atlantic polar lows associated with future climate warming. *Nature*, **467**, 309–312, doi:10.1038/nature09388.

Zappa, G., L. C. Shaffrey, K. I. Hodges, P. G. Sansom, and D. B. Stephenson, 2013: A multimodel assessment of future projections of North Atlantic and European extratropical cyclones in the CMIP5 climate models. *J. Climate*, **26**, 5846–5862, doi:10.1175/JCLI-D-12-00573.1.

——, ——, and ——, 2014: Can polar lows be objectively identified and tracked in the ECMWF operational analysis and the ERA-Interim reanalysis? *Mon. Wea. Rev.*, **142**, 2596–2608, doi:10.1175/MWR-D-14-00064.1.